

# Lidar measurements taken with a large-aperture liquid mirror. 2. Sodium resonance-fluorescence system

P. S. Argall, O. N. Vassiliev, R. J. Sica, and M. M. Mwangi

Sodium resonance-fluorescence lidar is an established technique for measuring atmospheric composition and dynamics in the mesopause region. A large-power-aperture product ( $6.6\text{-W m}^2$ ) sodium resonance-fluorescence lidar has been built as a part of the Purple Crow Lidar (PCL) at The University of Western Ontario. This sodium resonance-fluorescence lidar measures, with high optical efficiency, both sodium density and temperature profiles in the 83–100-km region. The sodium lidar operates simultaneously with a powerful Rayleigh- and Raman-scatter lidar ( $66\text{ W m}^2$ ). The PCL is thus capable of simultaneous measurement of temperature from the tropopause to the lower thermosphere. The sodium resonance-fluorescence lidar is shown to be able to measure temperature to an absolute precision of 1.5 K and a statistical accuracy of 1 K with a spatial-temporal resolution of 72 (km s) at an altitude of 92 km. We present results from three nights of measurements taken with the sodium lidar and compare these with coincident Rayleigh-scatter lidar measurements. These measurements show significant differences between the temperature profiles derived by the two techniques, which we attribute to variations in the ratio of molecular nitrogen to molecular oxygen that are not accounted for in the standard Rayleigh-scatter temperature analysis. © 2000 Optical Society of America

OCIS codes: 010.0010, 010.3640.

## 1. Introduction

Active remote sensing with lidar has proved to be one of the most important techniques for routine measurement of temperature in the middle atmosphere. Rayleigh-scatter systems are relatively simple and can make useful measurements in the upper stratosphere and mesosphere. However, the atmospheric density becomes sufficiently low at altitudes above 80 km that most Rayleigh-scatter lidars must integrate for periods of hours to obtain useful measurements. Furthermore, the interpretation of the temperature measurements at the greatest altitudes is complicated by the requirements for a seed temperature or pressure to begin the integration by use of the Ideal Gas law to convert relative density measurements into absolute temperatures. An advantage of the sodium temperature lidar is that the kinetic temperature is retrieved to a high degree of accuracy, without the need for a seed temperature.<sup>1</sup>

Temperatures derived from sodium resonance-fluorescence measurements both complement and extend the scientific applications of the Rayleigh-scatter temperature measurements. At altitudes of 83–100 km (where a sufficient amount of sodium is present), a typical sodium temperature lidar with a power-aperture product of  $1\text{ W m}^2$  has an equivalent Rayleigh-scatter power-aperture product of  $2 \times 10^4\text{ W m}^2$  at an altitude of 92 km, which is a Rayleigh-scatter power-aperture product approximately 300 times larger than those obtained with current large systems,<sup>2</sup> such as the Purple Crow Rayleigh-Scatter Lidar.

The disadvantages of the sodium technique are its complexity and limited altitude range. The complexity of the laser systems that generate narrow-band, tunable sodium light is considerably more than that of the relatively simple turn-key Nd:YAG lasers typically used with Rayleigh-scatter lidars. Also, the altitude range of the sodium layer is only approximately 15–20 km, with the densities (and hence the signal-to-noise ratio of the measurements) degrading considerably on the bottom and top sides of the layer.

There is a considerable advantage in having both a sodium temperature lidar and a Rayleigh-scatter lidar collocated and operating simultaneously. The sodium temperature lidar is able to obtain high temporal-spatial measurements of temperature in

---

The authors are with the Department of Physics and Astronomy, University of Western Ontario, London, Ontario N6A 3K7, Canada. The e-mail address for P. S. Argall is sargall@physics.uwo.ca.

Received 31 August 1999; revised manuscript received 4 February 2000.

0003-6935/00/152393-08\$15.00/0

© 2000 Optical Society of America



$D_{2\alpha}$  line. Once this has been achieved the operations of locking the laser to the selected spectral features and jumping between them becomes fully automatic. The sodium-control PC locates and then zooms in on the selected fine-structural features of the DFSS. It then locks to each selected feature in turn and controls the lidar data acquisition to ensure that atmospheric backscatter measurements taken at each wavelength are recorded separately. Status information, including locking frequency and accuracy, is continuously sent to the lidar data acquisition PC and recorded along with the atmospheric backscatter measurements.

The program that controls the sodium-control PC has adaptive features that allow it to learn and to adapt to the changing characteristics of the RDL. As the RDL runs, the time required for switching the laser from one wavelength to the next becomes shorter. After several minutes of operation the time required for switching the RDL wavelength between spectral features of the DFSS is less than 5 s. The control program usually recovers automatically from serious mode hops of the laser. In cases when recovery cannot be achieved automatically, the operator is alerted.

Locking the laser frequency to the fine-structural features of the DFSS is achieved by scanning of the laser output through a frequency range of  $\pm 4$  MHz, centered about a previously determined position of the spectral feature. During the scanning, which is repeated ten times to improve the signal-to-noise ratio, the intensity of the fluorescence from the sodium cell is recorded as a function of laser output frequency. A parabola is then fitted to these measurements, and the extrema of the parabola are used to determine any error of the central frequency of the laser scan from the extrema of the spectral feature. The central frequency of the laser scan is then updated so it corresponds to the spectral feature, and the process is repeated. This procedure compensates for drift in the laser, which generally occurs at a rate of only a few megahertz per minute. Although the laser is scanned over a frequency range of 8 MHz to permit locking (discussed further in Subsection 5.C.2 below), this has no significant effect on the calculated atmospheric temperatures.

An analysis of the status information produced by the locking program for the night of 21 May 1998 shows that, during 4 h and 50 min of operation, in only two of 1,038,000 attempts was the procedure unable to determine the location of the selected spectral feature. On both occasions the system automatically recovered, and no operator intervention was required. Adjustments made to the laser frequency by the locking program during this period show that, for the 1,038,000 times when the laser frequency was compared with a spectral feature of the DFSS, 78% of the time the agreement was within  $\pm 0.5$  MHz and 99.6% of the time it was within  $\pm 1.5$  MHz, corresponding to a temperature uncertainty of less than 0.16 K.

As the sodium lidar temperature retrieval is based on determining the Doppler broadening of the laser

**Table 1. Specifications of the Detector System of the Purple Crow Sodium and Rayleigh Lidars**

Parameter	PCL Sodium	PCL Rayleigh
Aperture	2.65-m diameter	2.65-m diameter
Focal length	5.175 m	5.175 m
Obscuration of the mirror	0.11	0.11
Field of view (full width)	0.39 mrad	0.39 mrad
Interference filter bandwidth	1.0 nm	1.0 nm
Height resolution	24 m	24 m
System efficiency	1.0%	1.2%

light backscattered from the atmosphere, it is necessary to know the spectral width of the transmitted laser pulses. Although the PDA is seeded by the RDL, its spectral output is significantly wider than the seed laser (the RDL) and may also be asymmetric. It is necessary, therefore, to measure the spectral shape of the PDA output. This measurement is made with a spectrum analyzer (Coherent Model 240) under control of the sodium-control PC. At predetermined intervals throughout an observation period, atmospheric backscatter measurements are halted while the spectral output of the PDA is measured. The sodium-control PC sets the transmission frequency of the spectrum analyzer and then measures the average intensity of the PDA pulse that is within the selected range. The sodium-control PC then steps the transmission frequency of the spectrum analyzer and measures the next pulse from the PDA. This process continued for  $\sim 20$  s until a full spectrum of the PDA output was measured.

### 3. Receiver System

The receiver system used for the measurements described in the present paper is the same as that described by Sica *et al.*<sup>3</sup> The primary collector for the detector system is a 2.65-m-diameter liquid-mirror telescope. A cooled photomultiplier (Hamamatsu R5600P-01) was used for photon detection. Table 1 summarizes the specifications of the PCL receiver system.

Nonlinearity in the detection system owing to pulse pileup and paralyzation effects are insignificant for the sodium system. The maximum detection rate measured at the peak of the sodium layer was  $\sim 4$  MHz, whereas the sodium detection system shows a measurable deviation from linearity above 6 MHz. Photomultiplier protection from low-level returns is provided by a high-speed rotating chopper. Photomultiplier gating is not used and thus was not a source of detector nonlinearity.

### 4. Density and Temperature Retrieval

The method used for the determination of temperature by the two-frequency sodium technique has been described in several places.<sup>1,11,13</sup> The measurements presented here were obtained by switching between two laser wavelengths every 600 laser shots (30 s), with range bins of 24 m.

The procedure by which the temperatures are de-

terminated is as follows: First, all data are visually inspected to permit any profiles that have obvious errors to be removed. Next, any measurements taken during a period when locking is lost or unstable are automatically discarded. The background, which is determined from the signal measured in the altitude range 60–75 km, is then removed from the measurements. The individual profiles are then normalized by use of the Rayleigh-scatter signal recorded by the sodium channel in the altitude range 35–55 km.<sup>1</sup> This procedure takes into account variations of instrumental parameters, such as laser power, and transmission variations in the lower atmosphere. Sodium density is then determined from each scan, and a temperature is determined from the ratios of each pair of scans.

PDA spectra are measured approximately every 15–20 min throughout the observation period. For each pair of scans two temperatures are calculated, one based on the preceding PDA scan and one based on the following PDA scan. The final temperature for each scan is calculated as the weighted average of these two temperatures; the weights are inversely proportional to the time interval between the center of the scan pair and the time when the respective PDA spectrum is measured.

## 5. Error Analysis

Analyses of errors for the two-frequency narrow-band sodium lidar have been presented in several places.<sup>2,10,11,14,15</sup> The following analysis closely follows these previous studies.

### A. Statistical Uncertainties

The uncertainty in the photocounts owing to statistical fluctuations leads to an uncertainty in the derived temperatures. She *et al.*<sup>11</sup> give a simple method for determining the temperature uncertainty based on the number of photocounts. Using this method for typical PCL measurements gives a statistical uncertainty of 1 K with a spatial–temporal resolution of 72 (km s) at an altitude of 92 km.

### B. Geophysical Errors

Errors in derived temperatures are introduced by the radial velocity of the atmospheric-sodium atoms.<sup>11</sup> Inasmuch as vertical motions are typically very small, less than  $3 \text{ m s}^{-1}$ , the corresponding temperature error is less than 0.34 K. Variations in the atmospheric sodium density over the period of an individual temperature measurement can also cause an error in temperature.<sup>11</sup> For fluctuations of the order of 1% at 92 km the uncertainty is less than 1 K.

### C. Laser-Frequency Errors

It has been shown by She *et al.*<sup>11</sup> that an error of 10 MHz in the absolute laser frequency will lead to errors in temperature of 0.02 K for  $f_a$  and 1.1 K for  $f_c$ . The frequency error arises because of the variation of cross section with frequency and is calculated based on a systematic offset of the laser from the spectral feature. Frequency error has two sources: First,

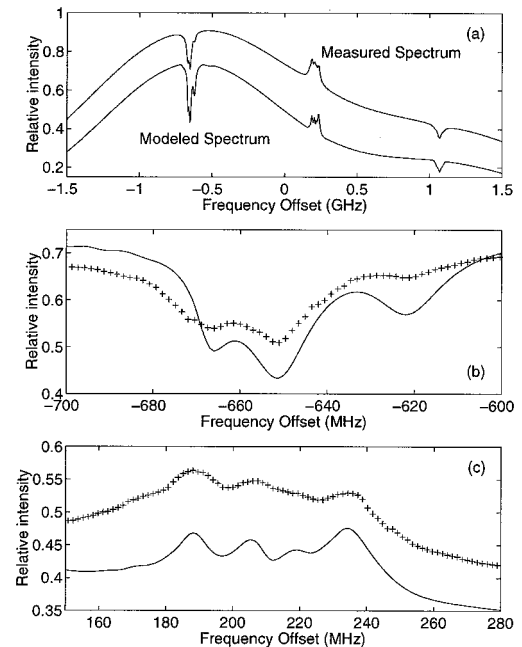


Fig. 2. Comparison of measured and modeled Doppler-free saturation spectra. (a) Measured spectrum offset vertically by +0.2 for clarity. (b) High-resolution spectrum of the  $f_a$  feature with no vertical offset. Modeled spectra are shown as solid curves; the individual measurements are shown as crosses. (c) Same as (b), except for the  $f_c$  feature.

knowledge of the absolute frequency of the Doppler-free features is critical; second, the ability of the control system to keep the laser frequency locked to the spectral feature must be known. We discuss these effects in the following two subsections.

### 1. Modeling of the Sodium Doppler-free Saturation Spectra

Papen *et al.*<sup>15</sup> have described a model for determining the absolute frequency of the Doppler-free features (DFF's) measured in the fluorescence spectrum from the sodium cell. A comparison of the measured spectrum with that produced by numerical simulation is shown in Fig. 2. In this figure the positions of the spectral features are shown to be in excellent agreement. Measured values of the physical properties of the sodium cell and the laser beam are used as input for the model. Some discrepancies in the amplitudes of the measured and the modeled spectra still exist, possibly because of absorption of the fluorescence within the cell. However, as noted by Papen *et al.*<sup>15</sup> this disagreement in intensity is not important, because only the frequency of the DFF's features is required. The agreement between the frequencies of measured and modeled DFF's is sufficiently good that the frequencies of the measured features are estimated to be known within an error of  $\pm 0.5$  MHz, i.e.,  $f_a = -651.5 \pm 0.5$  MHz and  $f_c = +188.2 \pm 0.5$  MHz. The uncertainties in these frequencies correspond to uncertainties in derived temperatures of  $6 \times 10^{-5}$  and 0.053 K, respectively.

**Table 2. Summary of Laser Locking Accuracy during the 4-h 31-min Observation Period on 21 May 1998**

Locking Feature	$f_a$	$f_c$
Number of laser DFSS comparisons	569,400	468,600
Occurrence (%) of laser frequency error of		
<0.5 MHz	85.2	68.8
<1.5 MHz	99.6	99.7
<2.5 MHz	99.9	99.9
<4.5 MHz	100	100

## 2. Laser Locking To Spectral Features

We define  $f_a$  and  $f_c$  as being at the center of the local extrema located at  $-651.5$  and  $+188.2$  MHz from the mean of the sodium  $D_{2\alpha}$  line.<sup>11</sup> These positions are chosen to facilitate the locking of the laser to these features, because a turning point in the spectrum provides a well-defined structural feature whose position is virtually independent of changes in system parameters such as laser power and cell temperature. Being able to monitor the locking procedure in real time and to track the turning point both gives a high degree of confidence in the reliability of the locking and enables the locking error to be determined accurately. Using a turning point as the locking point requires a high signal-to-noise ratio measurement of the spectrum because the rate of intensity change with frequency passes through zero at this point. The measured spectra shown in Fig. 2 are sampled once at each frequency. The spectra measured during active locking of the laser are sampled ten times at each frequency, enabling the turning points to be located with even higher precision than is indicated in the figure.

With the active locking scheme described above, the laser is scanned 4 MHz to either side of the spectral features. At both frequencies  $f_a$  and  $f_c$  the sodium cross section varies monotonically and can be considered linear over the small scanning range used. Therefore the cross section averaged over the laser scanning range will be close to the cross section at the central frequency of the laser scan, so scanning the laser in this way will not lead to significant systematic error in the calculated atmospheric temperature. The status information from the locking procedure for the 4 h and 50 min of observations on the night of 21 May 1998 is summarized in Table 2. This table shows that for most ( $>99.9\%$ ) of the time during this observation period the error in the laser frequency was less than 2.5 MHz. This error of 2.5 MHz is the dominant source of error in the laser frequency and leads to temperature errors at 200 K of 0.0015 K for  $f_a$  and 0.26 K for  $f_c$ .

### D. Uncertainty in the Transmitted Line Shape

The cross section of the sodium  $D_{2\alpha}$  line varies significantly over the frequency range of the PDA output pulses' spectral width. Thus it is necessary to know the spectral shape of the PDA output to be able to calculate the atmospheric temperature. Measure-

**Table 3. Summary of Instrumental and Geophysical Error Sources in PCL Na Temperatures**

Error Source	Magnitude (K)
Laser frequency ( $f_a$ ) absolute DFF frequency	$6 \times 10^{-5}$
Laser frequency ( $f_a$ ) laser locking to DFF feature	$1.5 \times 10^{-3}$
Laser frequency ( $f_c$ ) absolute DFF frequency	0.053
Laser frequency ( $f_c$ ) laser locking to DFF feature	0.26
Laser linewidth	0.9
<b>Total instrumental error</b>	<b>0.94</b>
Atmospheric-sodium radial velocity	0.34
Atmospheric and sodium density variations	1
<b>Total geophysical error</b>	<b>1.1</b>

ments of the spectrum of the PDA are taken every 15–20 min during observation periods. In the current configuration, taking a PDA spectrum requires that atmospheric observations stop for a period of  $\sim 20$  s while the spectrum is measured. From these measured spectra the spectral width of the PDA has been determined to be  $106 \pm 5$  MHz. From the method of analysis of Papen *et al.*,<sup>15</sup> the uncertainty in the calculated atmospheric temperature owing to the uncertainty in the PDA spectral width is 0.9 K. Planned improvements to the PDA spectral measurement system will significantly reduce this uncertainty in future measurements.

### E. Error Summary

Table 3 summarizes the errors in the temperatures calculated from the measurements made with the PCL sodium lidar system. The total instrumental systematic error is 0.94 K, and it is dominated by the error in the measurement of the laser linewidth. Geophysical systematic errors total 1.1 K, mainly because of possible sodium density fluctuations. Thus the accuracy of the PCL sodium lidar temperature measurements is  $\sim 1.5$  K.

## 6. Initial Scientific Results

A comparison of coincident mesopause temperature measurements made with the PCL sodium lidar and the PCL Rayleigh lidar on three nights has shown significant differences between the measurements and model atmospheres. The three nights were selected based on the high signal level and the uniformity of the sodium density on those nights. Selecting measurements with high signal levels ensures that the uncertainties in the derived temperatures are as small as possible, which is particularly important for the Rayleigh temperatures. Using measurements that do not exhibit any significant variations in sodium density ensures that density fluctuations do not significantly influence the sodium temperatures.

The altitude–time distribution of sodium concentration measured from 0249 to 0648 UT on 27 April 1998 is shown in Fig. 3. These measurements were taken 1 min apart with 24-m vertical resolution and have been smoothed by 3's and 5's (Ref. 16) in both

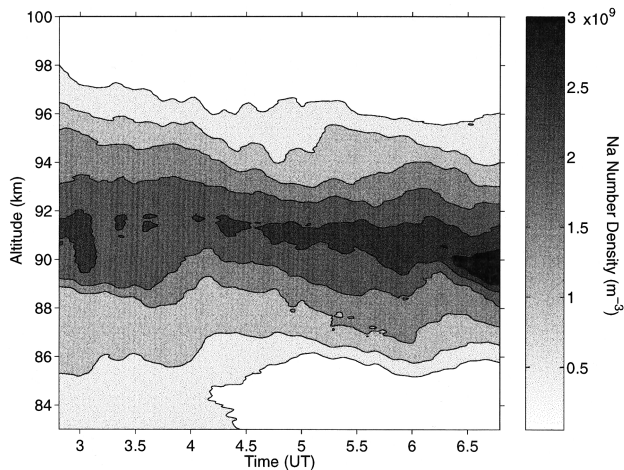


Fig. 3. Sodium number density measurements made with the PCL on 27 April 1998 from 0320 to 0648 UT. The measurements have a time resolution of 1 min and a range resolution of 24 m and are smoothed by 3's and 5's in both time and altitude.

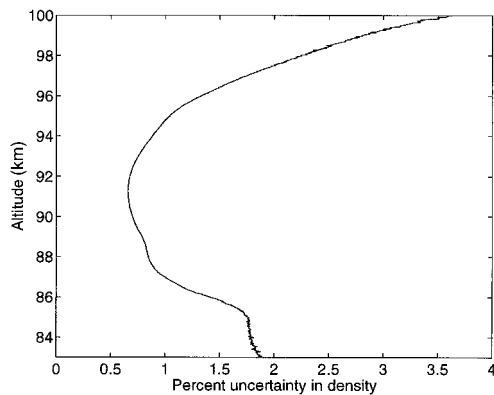


Fig. 4. Average statistical uncertainties for the sodium densities shown in Fig. 3. Variations from this average are generally less than 20%.

time and height. The statistical uncertainties associated with these density profiles are shown in Fig. 4.

Temperatures derived from the same measurements are shown in Fig. 5. These temperatures were calculated every minute for altitude bins of 24 m. These temperatures have been coadded to 250 m and 8 min and then smoothed with 3's and 5's in both altitude and time. The uncertainties associated with the temperatures presented in Fig. 5 owing to photon-counting statistics are shown in Fig. 6. The temporal and spatial variations in temperature highlight the variability in this region of the atmosphere that is due to atmospheric waves. For example, the temperature change at an altitude of 94 km during the period from 0320 to 0500 UT is  $\sim 18$  K.

Comparisons of the temperatures derived from the PCL Rayleigh and the sodium lidar systems are presented in Figs. 7–9. Temperatures from the Fleming model<sup>17</sup> for the appropriate date and latitude are included for reference. The Rayleigh and sodium temperatures shown in these figures are derived from

measurements taken over the same period. First, Rayleigh photocount profiles are coadded over the entire period (see figure captions), and then the Rayleigh temperature algorithm is seeded such that the uppermost temperature is equal to the corresponding sodium lidar temperature.

There are significant differences between the PCL lidar temperature profiles and the Fleming model. A climatology of the temperature of the mesopause region at mid-latitudes has been presented by Yu and She.<sup>18</sup> This climatology shows that the model is generally too cold in the mesopause region and lacks some of the detail in the structure of the temperature profile that actually exists, similar to the temperatures measured on 27 April and 21 May 1999 (Figs. 7 and 8).

The two methods of temperature measurement show general agreement in their overall magnitude and shape; however there are significant differences

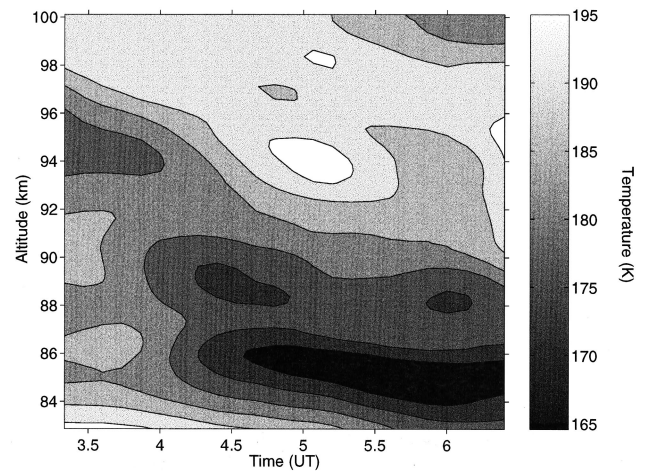


Fig. 5. Temperature measurements made with the PCL sodium lidar on 27 April 1998 from 0320 to 0624 UT. The temporal resolution of the measurements is 8 min, and the spatial resolution is 250 m. The measurements are smoothed with 3's and 5's in both time and altitude.

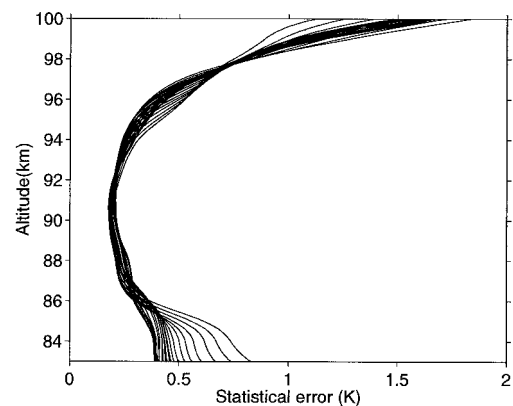


Fig. 6. Statistical uncertainties associated with the temperatures in Fig. 5. Each of the 24 curves represents the statistical uncertainty of an individual temperature profile used in the construction of Fig. 5.

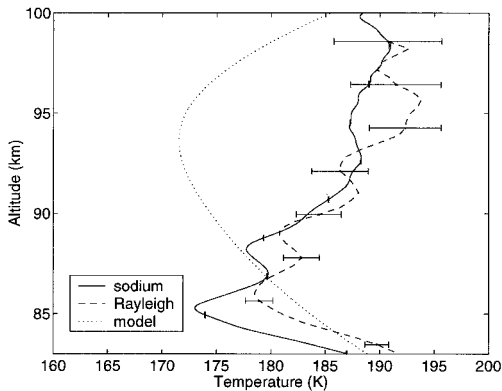


Fig. 7. Average temperature measured by the PCL sodium and Rayleigh lidar systems on 27 April 1998 during the period 0245 to 0652 UT. Also shown is the Fleming model. The error bars show  $1\sigma$  statistical uncertainties.

between the Rayleigh and the sodium lidar temperatures, particularly for 21 and 24 May 1998. A possible reason for the differences between the temperatures measured with the Rayleigh lidar and those measured with the sodium lidar is changes in atmospheric composition above 80 km. Mwangi *et al.*<sup>7</sup> discuss those differences in detail, in addition to presenting molecular-nitrogen and -oxygen densities derived from the PCL measurements. Mwangi *et al.* showed that the differences in the measured temperatures are consistent with previous measurements of the variations in the ratio of molecular nitrogen to molecular oxygen in this region of the atmosphere. The temperature differences measured with the sodium and Rayleigh lidar systems are small enough that a high-power-aperture-product lidar is required for such measurement, which one can then use to deduce the composition ratio of molecular nitrogen to molecular oxygen.

## 7. Summary and Conclusions

The Purple Crow Lidar now has the capability to make simultaneous Rayleigh-scatter and sodium res-

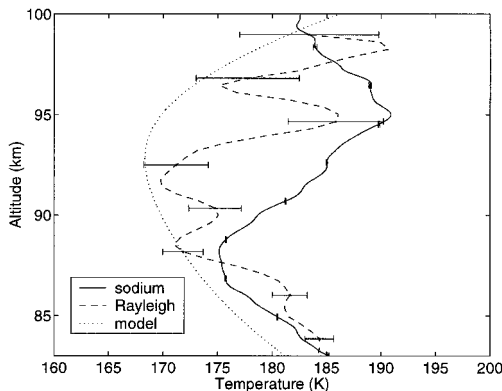


Fig. 8. Average temperature measured by the PCL sodium and Rayleigh lidar systems on 21 May 1998 during the period 0413 to 0844 UT. Also shown is the Fleming model. The error bars show  $1\sigma$  statistical uncertainties.

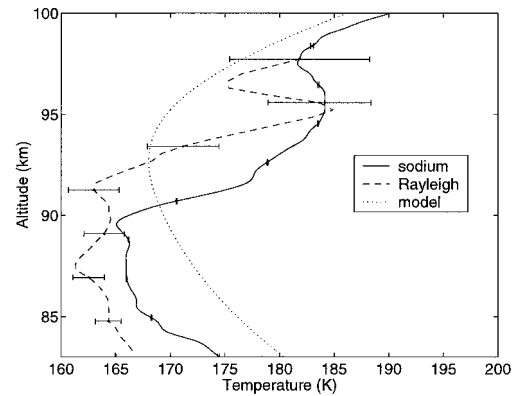


Fig. 9. Average temperature measured by the PCL sodium and Rayleigh lidar systems on 24 May 1998 during the period 0231 to 0835 UT. Also shown is the Fleming model. The error bars show  $1\sigma$  statistical uncertainties.

onance fluorescence measurements of temperature in the middle atmosphere. The sodium resonance fluorescence system has been shown to have the following features:

- (1) The Doppler-free saturation spectrum has been successfully modeled. The position of the lines is known to an equivalent temperature error of 0.03 K.
- (2) An automatic system has been built to measure the DFSS. The system can lock to a given feature in less than 5 s with an accuracy equivalent to a temperature uncertainty of 0.26 K.
- (3) An automatic system that uses a spectrum analyzer has been constructed to measure the line profile of the transmitted laser pulse. The system obtains a spectrum in  $\sim 20$  s, with uncertainties in the profile corresponding to a temperature uncertainty of 0.9 K.
- (4) The accuracy of temperature measurements at 92 km is 1.5 K, based on the above factors plus the sodium radial velocity error and the sodium density fluctuations.
- (5) Simultaneous Rayleigh-scatter and sodium resonance-fluorescence-temperature measurements made on three nights have been presented. Both techniques show significant differences from profiles expected from empirical model atmospheres.
- (6) The differences in temperature between the two techniques could be due to the assumption of a constant mean molecular mass in the retrieval of density and temperature from the Rayleigh-scatter system.

We thank the National Science and Engineering Research Council of Canada, the Meteorological Service of Canada, and the Centre for Research in Earth and Space Technology for their support of this project.

## References

1. C. Y. She, R. J. Alvarez II, L. M. Caldwell, and D. A. Krueger, "High-spectral-resolution Rayleigh-Mie lidar measurement of

- aerosol and atmospheric profiles," *Opt. Lett.* **17**, 541–543 (1992).
2. C. S. Gardner, D. C. Senft, T. J. Beatty, R. E. Bills, and C. A. Hostetler, "Rayleigh and sodium lidar techniques for measuring middle atmosphere density, temperature, and wind perturbations and their spectra," in *World Ionosphere/Thermosphere Study Handbook*, Scientific Committee on Solar Terrestrial Physics, eds. (International Council of Scientific Unions, Urbana, Ill., 1989), Vol. 2, pp. 148–187.
  3. R. J. Sica, S. Sargoytchev, P. S. Argall, E. F. Borra, L. Girard, C. T. Sparrow, and S. Flatt, "Lidar measurements taken through the use of a large-aperture liquid mirror. 1. Rayleigh-scatter system," *Appl. Opt.* **34**, 6925–6936 (1995).
  4. R. J. Sica and M. D. Thorsley, "Measurements of superadiabatic lapse rates in the middle atmosphere," *Geophys. Res. Lett.* **23**, 2797–2800 (1996).
  5. R. J. Sica and A. T. Russell, "Measurements of the effects of gravity waves in the middle atmosphere using parametric models of density fluctuations. I. Vertical wavenumber and temporal spectra," *J. Atmos. Sci.* **56**, 1308–1329 (1999).
  6. R. J. Sica, "Measurements of the effects of gravity waves in the middle atmosphere using parametric models of density fluctuations. II. Energy dissipation and eddy diffusion," *J. Atmos. Sci.* **56**, 1330–1343 (1999).
  7. M. M. Mwangi, R. J. Sica, and P. S. Argall, "Retrieval of molecular nitrogen and molecular oxygen densities in the upper mesosphere and lower thermosphere using ground-based lidar measurements," *J. Geophys. Res.* (to be published).
  8. A. Gibson, L. Thomas, and S. Bhattachacharyya, "Laser observation of ground-state hyperfine structure of sodium and of temperatures in the upper atmosphere," *Nature (London)* **281**, 131–132 (1979).
  9. K. H. Fricke and U. von Zahn, "Mesopause temperatures derived from probing the hyperfine structure of the D<sub>2</sub> resonance line of sodium by lidar," *J. Atmos. Terr. Phys.* **47**, 499–512 (1985).
  10. C. Y. She, H. Latifi, J. R. Yu, R. J. Alvarez II, R. E. Bills, and C. S. Gardner, "Two-frequency lidar technique for mesospheric Na temperature measurements," *Geophys. Res. Lett.* **17**, 929–932 (1990).
  11. C. Y. She, J. R. Yu, H. Latifi, and R. E. Bills, "High-spectral-resolution fluorescence light detection and ranging for mesospheric sodium temperature measurements," *App. Opt.* **31**, 2095–2106 (1992).
  12. M. A. White, D. Golias, D. A. Krueger, and C. Y. She, "A frequency-agile lidar for simultaneous measurement of temperature and radial wind in the mesopause region without sodium density contamination," in *Application to Lidar to Current Atmospheric Topics*, A. Sedlacek, ed., *Proc. SPIE* **2833**, 136–142 (1996).
  13. C. S. Gardner, D. G. Voelz, C. F. Christ, Jr., and A. C. Segal, "Lidar studies of the nighttime sodium layer over urbana, Illinois. 1. Seasonal and nocturnal variations." *J. Geophys. Res.* **91**, 13,659–13,673 (1986).
  14. R. E. Bills, C. S. Gardner, and C. Y. She, "Narrowband lidar technique for sodium temperature and Doppler wind observations of the upper atmosphere," *Opt. Eng.* **30**, 13–21 (1991).
  15. G. C. Papen, W. M. Pfenninger, and D. M. Simonich, "Sensitivity analysis of Na narrowband wind-temperature systems," *Appl. Opt.* **34**, 480–498 (1995).
  16. R. W. Hamming, *Design of Nonrecursive Filters* (Prentice-Hall, Englewood Cliffs, N.J., 1977), Chap. 6.
  17. S. Fleming, S. Chandra, M. Schoeberl, and J. Barnett, "Monthly mean global climatology of temperature, wind, geopotential height, and pressure for 0–120 km," *Tech. Memor. NASA TM-100697* (National Aeronautics and Space Administration, Washington, D.C., 1988).
  18. J. R. Yu and C. Y. She, "Climatology of a midlatitude mesopause region observed by a lidar at Fort Collins, Colorado (40.6N, 105W)," *J. Geophys. Res.* **100**, 6925–6936 (1995).